The EMBO Journal Vol. 22 No. 2 pp. 216–224, 2003

Absence epilepsy and sinus dysrhythmia in mice lacking the pacemaker channel HCN2

Andreas Ludwig[1,2], Thomas Budde[3], Juliane Stieber[1], Sven Moosmang[1], Christian Wahl[4], Knut Holthoff[5], Anke Langebartels[6], Carsten Wotjak[7], Thomas Munsch[3], Xiangang Zong[4], Susanne Feil[1], Robert Feil[1], Marike Lancel[6], Kenneth R.Chien[8], Arthur Konnerth[5], Hans-Christian Pape[3], Martin Biel[4] and Franz Hofmann[1]

[1]Institut für Pharmakologie und Toxikologie, Technische Universität München, D-80802 München, [3]Institut für Physiologie, Otto-von-Guericke Universität, D-39120 Magdeburg, [4]Department für Pharmazie, Ludwig-Maximilians Universität, D-81377 München, [5]Institut für Physiologie, Ludwig-Maximilians Universität, D-80336 München, [6]Schlafpharmakologie and [7]Mausverhalten/Neuronale Plastizität, Max-Planck-Institut für Psychiatrie, D-80804 München, Germany and [8]UCSD Institute of Molecular Medicine, La Jolla, CA 92093, USA

[2]Corresponding author
e-mail: ludwig@ipt.med.tu-muenchen.de

Hyperpolarization-activated cation (HCN) channels are believed to be involved in the generation of cardiac pacemaker depolarizations as well as in the control of neuronal excitability and plasticity. The contributions of the four individual HCN channel isoforms (HCN1–4) to these diverse functions are not known. Here we show that HCN2-deficient mice exhibit spontaneous absence seizures. The thalamocortical relay neurons of these mice displayed a near complete loss of the HCN current, resulting in a pronounced hyperpolarizing shift of the resting membrane potential, an altered response to depolarizing inputs and an increased susceptibility for oscillations. HCN2-null mice also displayed cardiac sinus dysrhythmia, a reduction of the sinoatrial HCN current and a shift of the maximum diastolic potential to hyperpolarized values. Mice with cardiomyocyte-specific deletion of HCN2 displayed the same dysrhythmia as mice lacking HCN2 globally, indicating that the dysrhythmia is indeed caused by sinoatrial dysfunction. Our results define the physiological role of the HCN2 subunit as a major determinant of membrane resting potential that is required for regular cardiac and neuronal rhythmicity.

Keywords: epilepsy/HCN channel/heart/membrane potential/pacemaker current

Introduction

Hyperpolarization-activated cation channels are found in a variety of cardiac cells and neurons (DiFrancesco, 1993; Pape, 1996). These channels activate in response to hyperpolarization to generate an inward current termed I_h. I_h has been proposed to contribute to the pacemaker depolarization which generates rhythmic activity in spontaneously active cardiac cells (DiFrancesco, 1993) and neurons (Pape, 1996; Luthi and McCormick, 1998). In addition, based on electrophysiological and pharmacological studies, it has been suggested that I_h channels may act as determinants of neuronal excitability (Pape, 1996) and plasticity (Mellor *et al*., 2002). It is well established that a number of other ion channels contribute to the above-mentioned functions. However, the specific physiological relevance of I_h to these functions remained unknown. For example, the role of I_h channels in pacemaking activity, especially of the sinoatrial node, is controversial. It has been argued that these channels do not contribute to cardiac automaticity for several reasons (Vassalle, 1995; Noma 1996; Miake *et al*., 2002). The main argument against a role for I_h channels has been their activation threshold which overlapped only slightly with the maximum diastolic potential (Vassalle, 1995; Shinagawa *et al*., 2000). Furthermore, available I_h channel blockers such as Cs^+ or zatebradine (UL-FS 49) may also inhibit other ion channels such as inward rectifiers and delayed rectifiers in the concentrations necessary to block I_h (Thompson *et al*., 2000; Satoh and Yamada, 2002). Hence, direct *in vivo* evidence for the physiological role of I_h channels has been lacking.

We and others recently identified a family of four homologous hyperpolarization-activated cation channels, termed HCN1–4, by molecular cloning (Clapham, 1998; Ludwig *et al*., 1998, 1999; Santoro *et al*., 1998; Ishii *et al*., 1999; Seifert *et al*., 1999). While all four HCN channels generate currents exhibiting the general features of native I_h, the contribution of the individual isoforms to the proposed functions of I_h is not known.

To address this question and to clarify the physiological role of I_h *in vivo*, we generated mice lacking the HCN2 isoform. HCN2-deficient mice were viable but smaller than their wild-type littermates. They exhibited reduced locomotor activity and spontaneous absence seizures. In addition, these mice showed pronounced cardiac sinoatrial dysrhythmia. Our results reveal that the I_h current generated by HCN2 channels critically determines the resting membrane potential of neurons and cardiac pacemaker cells. We demonstrate that HCN2 channels play a crucial role in the normal rhythmicity of thalamocortical relay neurons and sinoatrial myocytes.

Results and discussion

Disruption of the HCN2 gene

We disrupted the HCN2 gene through homologous recombination using a Cre/loxP-based strategy (Figure 1A). We deleted exons 2 and 3 encoding five of the six

transmembrane segments of the HCN2 channel including part of the pore. Heterozygous matings produced wild-type, HCN2$^{+/-}$ and HCN2$^{-/-}$ mice at the expected Mendelian ratio (Figure 1B). The deletion of the HCN2 gene was confirmed by northern blot analysis (Figure 1C). Immunoblotting of brain membrane proteins using an HCN2-specific antibody revealed that the protein is absent in HCN2$^{-/-}$ mice (Figure 1D). Northern blot analysis indicated that the global expression of the three remaining HCN channel family members HCN1, HCN3 and HCN4 in brain was not affected by the absence of HCN2 (Figure 1E). The brain morphology of HCN2$^{-/-}$ mice appeared normal as judged by analysis of cresyl violet-stained serial sections (data not shown). Homozygous mutant mice were smaller than their littermates (weight at 8 weeks; HCN2$^{+/+}$, 26.5 ± 1.1 g, n = 16; HCN2$^{-/-}$, 15.3 ± 0.5 g, n = 14; $P < 0.001$). In addition, HCN2$^{-/-}$ mice showed a whole-body tremor and were hypoactive.

I_h is nearly absent in HCN2$^{-/-}$ thalamocortical neurons

The loss of functional HCN2 channels was examined by whole-cell voltage clamp analysis of I_h in thalamic and hippocampal neurons. Wild-type thalamocortical relay

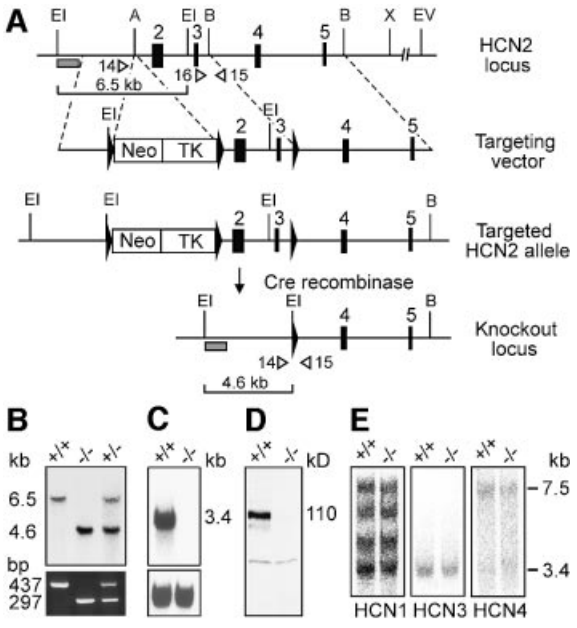

Fig. 1. Disruption of the HCN2 gene. (**A**) Top: wild-type HCN2 locus and targeting vector. Exons 2–5 are represented by black boxes. The targeting vector contains a *neo/tk* cassette flanked by two loxP sequences (black triangles) inserted in intron 1 and a third loxP site inserted in intron 3. A, *Acc*65I; B, *Bam*HI; EI, *Eco*RI; EV, *Eco*RV; X, *Xho*I. Bottom: homologously recombined allele and knockout locus after Cre-mediated deletion of exons 2 and 3 including the *neo/tk* cassette in embryonic stem cells. (**B**) Analysis of genomic DNA from HCN2$^{+/+}$, HCN2$^{+/-}$ and HCN2$^{-/-}$ mice. Top: Southern blot of *Eco*RI-digested DNA hybridized with the probe shown in (A) (shaded box). The 6.5 and 4.6 kb fragments represent the wild-type and mutant HCN2 allele, respectively. Bottom: multiplex PCR analysis using primers 14, 15 and 16 (open arrowheads in A) giving a 437 bp product for wild-type and 297 bp for the knockout allele. (**C**) Top: northern analysis using brain mRNA and a HCN2 probe. Bottom: blot hybridized with a β-actin probe. (**D**) Western analysis of brain membrane proteins using an anti-HCN2 antibody demonstrates the absence of HCN2 protein (110 kDa) in HCN2$^{-/-}$ mice. (**E**) Northern blot with brain mRNA hybridized with probes directed against HCN1, HCN3 and HCN4.

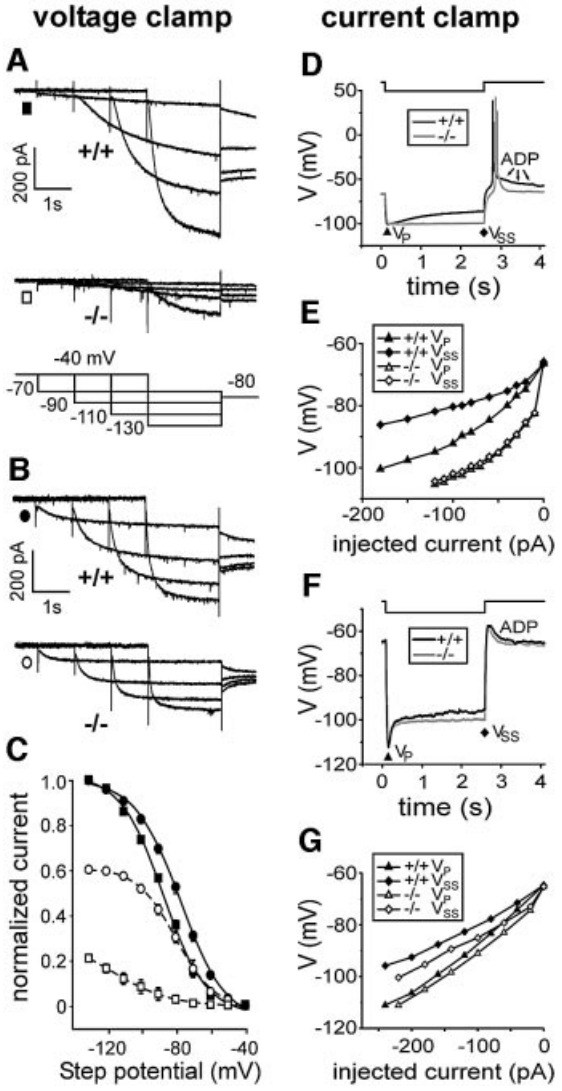

Fig. 2. I_h in thalamocortical and hippocampal CA1 neurons measured under voltage-clamp (left column) and current-clamp (right column) conditions. (**A**) I_h traces measured in thalamocortical neurons of wild-type and HCN2$^{-/-}$ mice. Neurons were voltage clamped for the times indicated from –40 mV to a range of test potentials followed by a step to –80 mV. (**B**) Currents of CA1 pyramidal cells generated in response to the step protocol indicated in (A). (**C**) Activation curves determined by tail current analysis of thalamocortical neurons (squares) and CA1 pyramidal cells (circles) from wild-type (filled symbols, solid lines) and HCN2 knockout mice (open symbols, dashed lines). Tail current amplitudes from HCN2$^{-/-}$ neurons were normalized to the maximal current measured in corresponding wild-type neurons. (D–G) Comparison of time-dependent anomalous rectification. (**D** and **F**) Superimposed negative voltage deviations (wild-type, black line; HCN2 knockout, grey line) evoked by a negative current step in thalamic relay (D) and hippocampal CA1 (F) neurons. The voltage step represents –180 pA for a wild-type and –80 pA for an HCN2$^{-/-}$ relay neuron (D), and –240 pA for a wild-type and –220 pA for a HCN2$^{-/-}$ pyramidal cell (F). The membrane potential of HCN2$^{-/-}$ cells was set to around –65 mV by current injection. ADP, after depolarization. (**E** and **G**) Peak voltage V_P (wild-type, closed triangles; knockout, open triangles) and steady-state voltage V_{SS} (wild-type, closed diamonds; knockout, open diamonds)–current relationships of thalamic relay (E) and CA1 pyramidal (G) neurons. The 'voltage sag' was determined by the difference between V_P and V_{SS}. Data in (E) were derived from seven wild-type and eight knockout cells; and those in (G) from four wild-type and four knockout cells.

neurons displayed a prominent I_h (Figure 2A; current at –50 mV, –5 ± 1 pA; –90 mV, –140 ± 17 pA; –130 mV, ~401 ± 32 pA; n = 9). Tail current analysis revealed a $V_{1/2}$ value of –88 ± 1 mV (Figure 2C). Thalamocortical neurons from HCN2$^{-/-}$ mice showed a dramatic reduction of I_h [Figure 2A; current (% of wild-type) at –50 mV, 0 ± 0.5 pA (0%); –90 mV, –16 ± 3 pA (11%); –130 mV, –84 ± 11 pA (21%); n = 11; $P < 0.001$ for all potentials]. This residual current activated at more hyperpolarized potentials, resulting in a $V_{1/2}$ of –115 ± 4 mV.

In HCN2-deficient CA1 pyramidal cells (Figure 2B and C), I_h was reduced by only about one-third as compared with wild-type (current amplitude at –130 mV: –326 ± 20 pA for HCN2$^{+/+}$ mice, n = 7; –198 ± 12 pA for HCN2$^{-/-}$ mice, n = 8; $P < 0.001$). In these cells, the voltage dependence of activation was not significantly different between both genotypes [$V_{1/2}$: –78 ± 1 mV and –80 ± 1 mV for HCN2$^{+/+}$ mice (n = 13) and HCN2$^{-/-}$ mice (n = 11), respectively]. I_h in CA1 pyramidal cells from HCN2$^{-/-}$ mice consistently activated more rapidly compared with wild-type mice. For example, at a potential of –130 mV, τ_{act} was 100 ± 5 ms (n = 7) and 83 ± 3 ms (n = 8) for wild-type and HCN2$^{-/-}$ mice, respectively. Perfusion with 100 μM 8-bromo-cAMP shifted the $V_{1/2}$ values of wild-type CA1 pyramidal neurons significantly in the positive direction (shift: +4 ± 0.5 mV, n = 6, $P < 0.001$). In contrast, cAMP induced no significant shift of the $V_{1/2}$ values of HCN2 knockout CA1 pyramidal cells (shift: +2 ± 1 mV, n = 4, P = 0.1). These results correspond well to the properties of heterologously expressed HCN channels (Ludwig *et al.*, 1998; Santoro *et al.*, 1998). Recombinant murine HCN1 channels activate significantly more rapidly than HCN2 channels. In addition, HCN2 channels display a pronounced shift (+13 mV) in the steady-state activation curve in response to cAMP, whereas murine HCN1 channels are only shifted minimally (+2 mV). Hence, the properties of I_h in HCN2-deficient CA1 pyramidal neurons closely resemble those of heterologously expressed HCN1 channels. Taken together, these results exclude the hypothesis that I_h in wild-type CA1 pyramidal cells is generated solely by HCN1 channels (Santoro *et al.*, 2000). Instead, our findings support the notion that I_h in these neurons is produced by co-expressed HCN1 and HCN2 subunits. In addition, our results are in agreement with the known expression pattern of HCN channel transcripts (Moosmang *et al.*, 1999; Santoro *et al.*, 2000) and suggest that in contrast to hippocampal CA1 neurons, I_h in thalamocortical cells is generated predominantly by HCN2.

The voltage sag and afterdepolarization following hyperpolarization in thalamocortical neurons is mediated by HCN2 channnels

One hallmark of I_h current activation during current clamp recordings is a depolarizing voltage sag generated during the course of negative voltage deviations (Pape, 1996). Therefore, time-dependent rectification was analysed under current clamp conditions by applying hyperpolarizing current injections (Figure 2D–G). Thalamic relay neurons from wild-type mice revealed both a prominent slow time-dependent rectification during hyperpolarization and a burst of action potentials riding on top of a low-threshold calcium spike following release from hyperpolarization (Figure 2D). With hyperpolarizations reaching a membrane potential of ~–100 mV, the amplitude of the voltage sag was 9.0 ± 1.2 mV (n = 7; Figure 2E). Typically the low-threshold calcium spike was followed by an afterdepolarization (ADP; see Luthi and McCormick, 1998). Both the slow time-dependent rectification and the ADP were abolished by 1 mM Cs$^+$ (n = 4). In contrast, only a very small voltage sag (1–2 mV) and basically no ADP could be observed in relay neurons from HCN2 knockout mice for hyperpolarizations reaching up to –115 mV (Figure 2D and E; n = 8). However, the generation of a typical low-threshold calcium spike

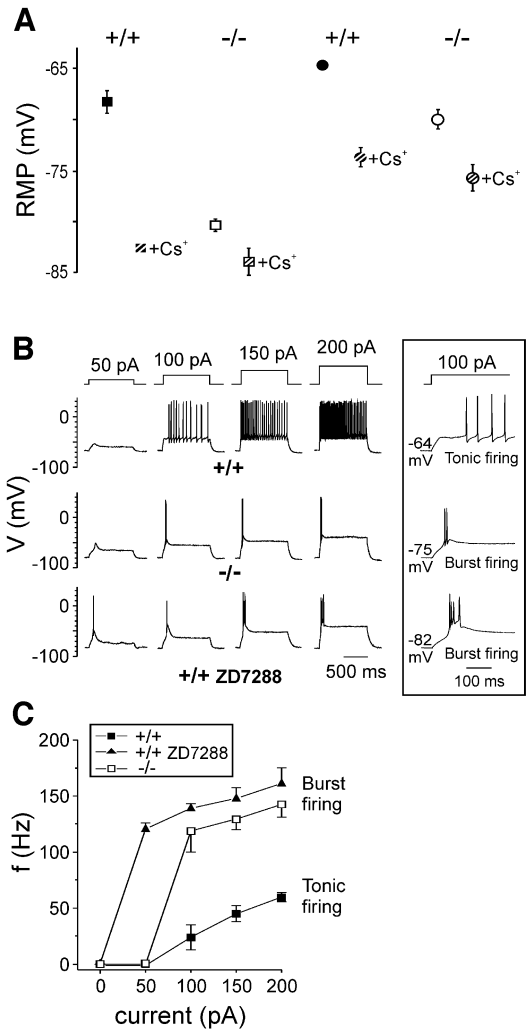

Fig. 3. Resting membrane potential and firing patterns of HCN2 knockout and wild-type neurons. (**A**) Resting membrane potentials of thalamocortical neurons (squares) and CA1 pyramidal cells (circles). Measurements under control conditions are indicated by filled (wild-type) and open (HCN2 knockout) symbols. Membrane potentials of these neurons measured after block of I_h with 1 mM Cs$^+$ are indicated by hatched symbols. Determination of membrane potentials after block of I_h with 100 μM ZD7288 led to identical results (see text). (**B**) Different intrinsic firing properties of wild-type and HCN2$^{-/-}$ thalamocortical neurons. Shown are the firing patterns elicited by 1 s depolarizing current pulses at resting membrane potential of wild-type, HCN2$^{-/-}$ and wild-type neurons in the presence of 100 μM ZD7288. The amount of current injected is indicated above. Inset: traces elicited by injection of 100 pA at an expanded time scale. (**C**) Frequency of action potential generation versus injected current. The frequency of action potentials was determined for the first 150 ms after the beginning of the depolarizing pulse.

including action potential bursting was not corrupted by the loss of HCN2 channels.

Other than for relay neurons, CA1 pyramidal cells from both wild-type and HCN2 knockout mice displayed a prominent voltage sag during hyperpolarizing steps and a short ADP following release from hyperpolarization (Figure 2F). Both voltage deviations were completely abolished by 1 mM Cs^+ ($n = 4$; data not shown). As expected from the faster time course of I_h activation in pyramidal cells, the time-dependent rectification was rapid. For hyperpolarizations reaching ~–105 mV, the amplitude of the voltage sag but not the rate of its rise were significantly different (Figure 2G).

Hyperpolarized resting membrane potential of HCN2$^{-/-}$ thalamocortical neurons

It has been suggested that I_h contributes to the resting membrane properties of thalamocortical neurons (McCormick and Pape, 1990). Hence, we examined the resting membrane potential (RMP) of these cells from wild-type and HCN2$^{-/-}$ mice. The RMP of HCN2-deficient thalamocortical cells was ~12 mV more hyperpolarized than that of wild-type cells (–68 ± 1 mV for HCN2$^{+/+}$ mice, $n = 6$; –80 ± 1 mV for HCN2$^{-/-}$ mice, $n = 9$; $P < 0.001$; Figure 3A). In accordance with these results, block of I_h by 1 mM Cs^+ and also by 100 μM ZD7288 led to a pronounced hyperpolarizing shift of the RMP of wild-type thalamocortical cells, whereas the RMP of HCN2$^{-/-}$ cells displayed only a minor additional hyperpolarization [RMP of HCN2$^{+/+}$ cells, –83 ± 1 mV ($n = 5$) and –83 ± 1 mV ($n = 8$); RMP of HCN2$^{-/-}$ cells, –84 ± 1 mV ($n = 5$) and –84 ± 2 mV ($n = 6$) in the presence of 1 mM Cs^+ and 100 μM ZD7288, respectively].

The RMP of HCN2-deficient hippocampal CA1 neurons was 5 mV more negative than that of wild-type cells (–65 ± 1 mV for HCN2$^{+/+}$, $n = 5$; –70 ± 1 mV for HCN2$^{-/-}$, $n = 5$; $P < 0.01$). These data demonstrate that HCN2 contributes importantly to the RMP of thalamocortical neurons and, to a lesser extent, to that of hippocampal neurons.

Burst rather than tonic firing mode from resting membrane potential in HCN2$^{-/-}$ thalamocortical neurons

Thalamocortical neurons generate action potentials in one of two distinct modes: burst firing mode, in which 2–8 action potentials are generated together as a high-frequency burst discharge triggered by the T-type calcium current, and tonic (or single spike) activity in which action potentials occur singly at lower frequency relatively independently of one another (reviewed in McCormick and Bal, 1997). We examined the intrinsic firing properties of thalamocortical neurons by whole-cell current clamp recordings. Injection of positive current into wild-type neurons at RMP resulted in the generation of tonic series of action potentials, the frequency of which was dependent on the stimulation strength (Figure 3B, upper trace; Figure 3C, $n = 6$). By comparison, thalamocortical neurons in HCN2$^{-/-}$ mice responded to the same depolarizing stimuli from RMP with stereotyped high-frequency burst discharges (Figure 3B, middle trace). The intra-burst frequency observed in HCN2$^{-/-}$ mice was significantly higher as compared with tonic firing in wild-type mice ($P < 0.001$). Similarly, application of 100 μM ZD7288 to wild-type thalamocortical neurons resulted in a hyperpolarizing shift of the RMP and an associated shift from the tonic to the burst firing mode (Figure 3B, bottom trace; Figure 3C, $n = 6$). The frequency of burst firing was not significantly different from that of HCN$^{-/-}$ neurons ($P = 0.4$). Taken together, these results demonstrate that the more hyperpolarized RMP in thalamocortical neurons lacking HCN2 channels leads to a pronounced alteration in the responsiveness of these neurons. The findings are in line with the idea that depolarizing inputs impinging at the RMP evoke high-frequency bursts of action potentials due

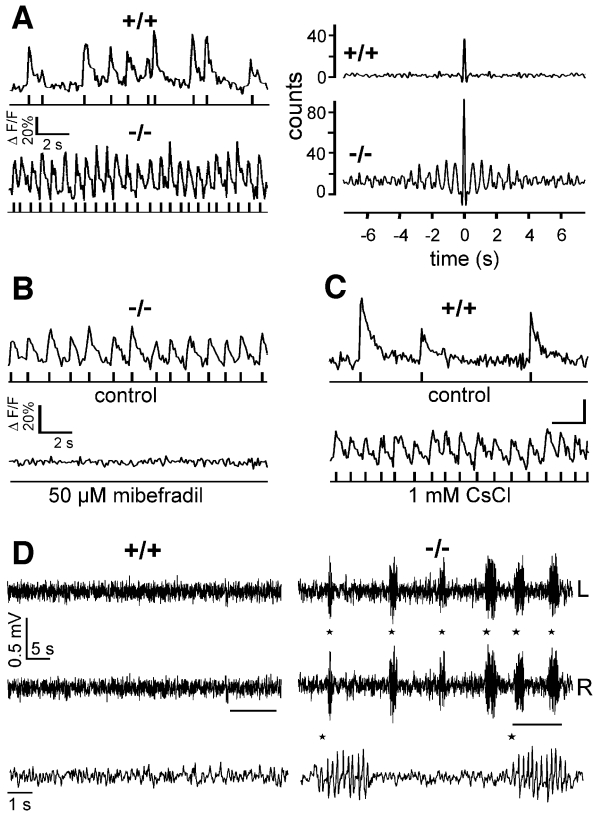

Fig. 4. Thalamic oscillatory activity and spike-and-wave discharges in HCN2$^{-/-}$ mice. (**A**) Comparison of spontaneous activity in thalamic neurons in brain slices from wild-type and HCN2$^{-/-}$ mice. Left: typical spontaneous calcium transients recorded with two-photon microscopy. Thalamic cells in wild-type slices showed irregular spontaneous activity (top left), whereas one-third of spontaneous active HCN2-deficient thalamic neurons showed oscillatory calcium transients (bottom left). Rasterplots below the original traces show the results from activity analysis. Each upward deflection in the calcium trace is represented by an individual time marker in the Rasterplot. Right: autocorrelograms of calcium transients shown left. Autocorrelograms quantify the oscillatory properties of these activities (König, 1994). (**B**) Oscillatory activity in thalamic cells of HCN2-deficient mice depends on activation of T-type calcium channels. The specific T-type calcium channel antagonist mibefradil blocks oscillatory activity in thalamic cells (top) in a concentration range between 2 and 50 μM (bottom). (**C**) Induction of oscillatory activity in thalamic cells of wild-type slices by block of HCN currents. In wild-type slices, irregular spontaneous activity (top) can be transferred into oscillatory activity by treatment with 1 mM CsCl (bottom). Calibration bars as in (B). (**D**) Comparison of spontaneous EEG patterns between wild-type and HCN2$^{-/-}$ mice. Representative 1 min EEG recordings (L, R; left, right channel). Spike-and-wave discharges are indicated by asterisks. The horizontal bars demarcate the traces shown on an expanded time scale below the 1 min recordings.

to activation of the T-type current in these neurons (McCormick and Bal, 1997).

Increased susceptibility to oscillations in HCN2$^{-/-}$ thalamocortical neurons

Burst firing in thalamocortical neurons is generally accepted to represent an important cellular substrate of synchronized oscillatory activity in thalamocortical circuits typically observed during sleep and generalized epilepsy (Steriade, 2000). To explore a potential oscillatory activity in the thalamus, we used two-photon microscopy in a network detection approach. This non-invasive technique allows changes in somatic calcium concentration to be recorded in several cells in parallel as a reporter for electrical activity (Mao *et al*., 2001). We used a thalamic slice preparation *in vitro* (Huguenard and Prince, 1994) in which oscillatory activity was facilitated through pharmacological means (Avoli *et al*., 1996). In wild-type slices, more than half of the cells (39/63) showed spontaneous calcium transients, reflecting action potential activity (Figure 4A, top left). In none of these cells was any oscillatory behaviour detected. In recordings from thalamic slices from HCN2$^{-/-}$ mice, a similar fraction of cells (36/67) were spontaneously active. In contrast to cells from wild-type mice, however, more than one-third of these spontaneously active cells (13/36) exhibited a prominent oscillatory activity, as expected for recurrent bursts of action potentials (Figure 4A, bottom). We tested if the oscillatory activity was dependent on T-type calcium channel activation by using mibefradil, a drug that selectively inhibits T-type calcium channels in micromolar concentrations (Lacinova *et al*., 2000; Martin *et al*., 2000). Mibefradil blocked oscillatory activity ($n = 5$ slices of three animals, Figure 4B) in a concentration range of 2–50 μM.

These results demonstrate that the lack of HCN2 facilitates the spontaneous occurrence of oscillatory activity in thalamocortical synaptic networks. This finding is supported further by the fact that in slices of wild-type animals, oscillatory cell activity could be induced by blocking HCN currents with 1 mM CsCl ($n = 5$ slices of three animals, Figure 4C).

Reduced locomotor activity and absence epilepsy

Several studies suggest that synchronized oscillations in the thalamocortical network play a central role in the genesis of absence seizures (Steriade *et al*., 1993; Huguenard, 1999; Kim *et al*., 2001). The behavioural phenotype of absence epilepsy in humans and mice is characterized by brief episodes of immobility (behavioural arrest) during seizure activity (Noebels *et al*., 1997). We studied the spontaneous behaviour of HCN2-deficient mice using an open-field test. Horizontal locomotion of mutant mice was significantly less than that of wild-type controls (63 ± 3 m for HCN2$^{+/+}$ mice, $n = 10$; 47 ± 4 m for HCN2$^{-/-}$ mice, $n = 7$; $P < 0.05$). Similarly, mutant mice reared less often. We then obtained epidural electroencephalographic (EEG) recordings from freely moving HCN2$^{-/-}$ mice and wild-type littermates. HCN2-deficient mice displayed frequent bilaterally synchronous spike-and-wave discharges (SWDs; Figure 4D), the hallmark of absence epilepsy. The SWDs had a frequency of 5 Hz and comprised 3 ± 1% ($n = 7$) of the light phase recording time, whereas no SWDs were observed in wild-type littermates ($n = 8$). The SWDs were accompanied by behavioural arrest of the animals. Administration of ethosuximide suppressed the occurrence of SWDs in mutant mice almost completely (percentage of total duration of SWDs in the first hour after i.p. administration at dark onset: 13.2 ± 5.1% for vehicle, 0.2 ± 0.1% for ethosuximide; $n = 4$, $P < 0.05$). Hence, HCN2-deficient mice reflect the typical clinical and pharmacological characteristics of generalized absence epilepsy.

Taken together, our results strongly support the following mechanism for the generation of absences seizures in HCN2$^{-/-}$ mice: the hyperpolarizing shift in the resting potential of HCN2-deficient thalamocortical relay neurons removes inactivation from T-type Ca^{2+} channels and thereby promotes low-threshold burst firing in response to depolarizing inputs (McCormick and Bal, 1997; Kim *et al*., 2001). This results in an increased oscillatory activity in the thalamocortical network contributing to seizure activity. It should be noted that additional influences, particularly of the cortex (Meeren *et al*., 2002) and intrathalamic nuclei (Seidenbecher *et al*., 2001), may also contribute to the observed SWDs.

Absence seizures in HCN2-deficient mice do not modulate the expression of other HCN channel genes

We investigated whether or not the presence or absence of absence seizures in HCN2$^{-/-}$ mice might alter the brain expression pattern of the remaining HCN isoforms

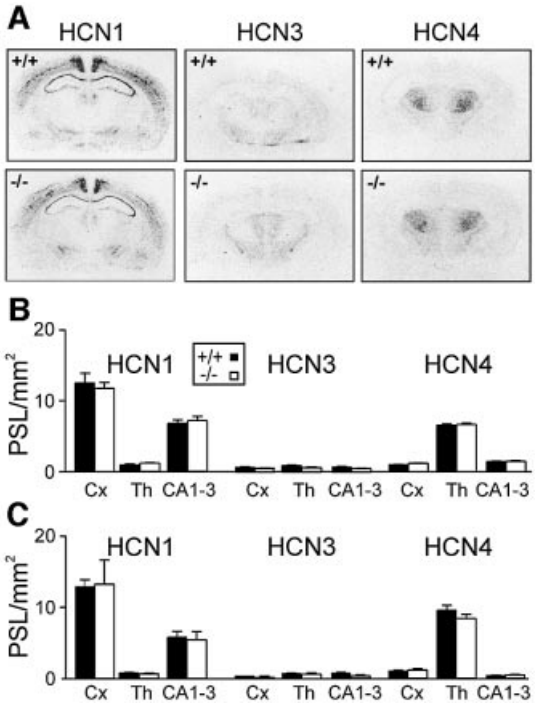

Fig. 5. Expression of HCN channel transcripts in wild-type and HCN2 knockout brain. (**A**) Autoradiograms of brain sections hybridized *in situ* with HCN1, HCN3 and HCN4 probes under control conditions. (**B**) HCN subunit expression under control conditions. HCN mRNA levels were quantified by analysis of phosphorimaged sections ($n = 6$–8 for each genotype and HCN isoform). PSL, photo-stimulated luminescence units; Cx, cortex; Th, thalamus; CA1–3, CA1–3 regions of the hippocampus. (**C**) HCN subunit expression after chronic application of ethosuximide over 4 weeks.

Table I. Heart rate and dysrhythmia in HCN2-deficient mice

Parameter	Genotype	Rest	Active	Isoproterenol	Atropine	Methoxamine
Heart rate (per min)	$HCN2^{+/+}$	531 ± 17	673 ± 6	727 ± 8	723 ± 12	311 ± 25
	$HCN2^{-/-}$	510 ± 9	677 ± 17	708 ± 15	692 ± 4	377 ± 28
SDRR (ms)	$HCN2^{+/+}$	7 ± 1	5 ± 2	4 ± 1	3 ± 1	46 ± 18
	$HCN2^{-/-}$	17 ± 1[a]	5 ± 7	3 ± 1	1 ± 0	34 ± 8

[a]Significant difference ($P < 0.001$) between corresponding values from wild-type and HCN2-deficient mice. SDRR, standard deviation of RR intervals representing a measure of dysrhythmia. Each group included six animals.

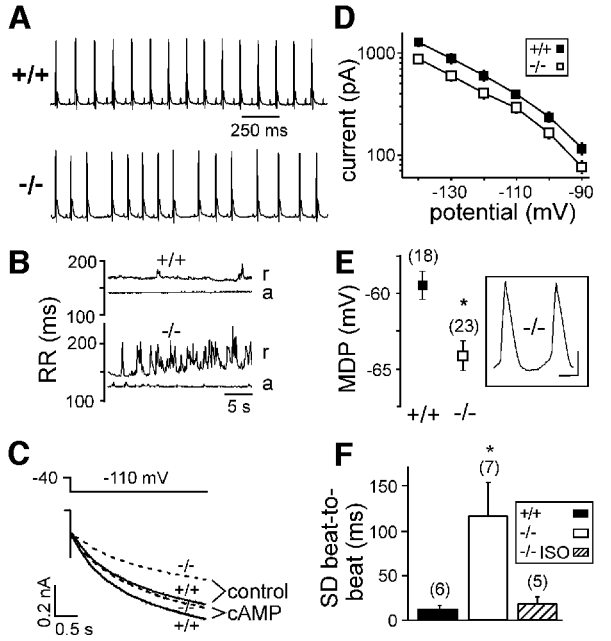

Fig. 6. Sinus dysrhythmia and sinoatrial I_h in HCN2-deficient mice. (**A**) Telemetric ECG recordings (lead II) obtained simultaneously from wild-type and HCN2-deficient mice at rest. (**B**) RR intervals from wild-type and HCN2-deficient mice at rest (r) and during spontaneous physical activity (a) plotted against time. (**C**) I_h in sinoatrial node cells. Averaged current traces from wild-type (solid lines) and $HCN2^{-/-}$ mice (dashed lines) under control conditions and in the presence of 100 μM cAMP in the pipette solution. (**D**) Characterization of I_h. Currents were evoked by 3 s pulses to a range of test potentials from a holding potential of –40 mV. Current amplitudes at the end of the pulse are plotted against the test potential (58 wild-type cells, 60 HCN2 knockout cells, $P < 0.05$ at all potentials). (**E**) Maximum diastolic potentials (MDPs) determined from action potentials of isolated sinoatrial node cells. The inset shows an example of action potentials recorded from an HCN2-deficient cell. Scale bars: 200 ms, 20 mV. *$P < 0.05$ versus wild-type. (**F**) Beating of isolated heart atria. The standard deviation (SD) of atrial beat-to-beat intervals is a measure of dysrhythmia. *$P < 0.05$ versus wild-type. ISO, isoproterenol. Mean beating frequency was not significantly different between the three groups.

compared with wild-type. We first determined the regional expression of HCN1, HCN3 and HCN4 transcripts in brain under control conditions by *in situ* hybridization. These experiments revealed no significant differences in the distribution pattern of the three isoforms between wild-type and HCN2-deficient mice (Figure 5A, $n = 6–8$ for each genotype and HCN isoform). Likewise, their relative expression levels in cortex, thalamus and hippocampus were unchanged (Figure 5B). We repeated these experiments with animals chronically treated with ethosuximide to suppress absence seizures in $HCN2^{-/-}$ mice. The expression of HCN1, HCN3 and HCN4 in $HCN2^{-/-}$ animals was not different from wild-type under these conditions (Figure 5C, $n = 6–8$ for each genotype and HCN isoform). These results indicate that neither the deletion of HCN2 nor the presence of absence seizures in $HCN2^{-/-}$ mice modulates the expression of the other HCN channels.

Cardiac sinus dysrhythmia

I_h has been proposed to play an important role in controlling cardiac pacemaking activity (DiFrancesco, 1993; Irisawa *et al*., 1993). However, this role has been questioned by several authors (Vassalle, 1995; Noma, 1996; Shinagawa *et al*., 2000; Miake *et al*., 2002). Two HCN genes are expressed in the murine sinoatrial node, HCN4 (high mRNA levels) and HCN2 (lower transcript levels; Moosmang *et al*., 2001). We examined $HCN2^{-/-}$ mice for possible alterations in cardiac rhythmic activity by electrocardiographic (ECG) telemetry. Mean heart rate at rest and during spontaneous activity was not different between wild-type and mutant mice (Table I). However, the intervals between successive heart beats of HCN2-deficient mice varied widely at rest (Figure 6A and B). Each QRS complex was preceded by a regular P wave in a normal PR interval, indicating that the dysrhythmia in HCN2-deficient mice is due to a dysfunction of the sinoatrial node. This sinus dysrhythmia of $HCN2^{-/-}$ mice was absent during phases of enhanced spontaneous activity (Figure 6B). Similarly, stimulation of cardiac β-adrenergic receptors by isoproterenol or block of muscarinic receptors by atropine increased the heart rate in wild-type as well as in knockout mice, and completely abolished the dysrhythmia (Table I). Conversely, administration of the α_1-adrenergic agonist methoxamine induced bradycardia through baroreflex stimulation following vasoconstriction (Wickman *et al*., 1998) in both wild-type and knockout mice (Table I). It has been proposed that the sympathetic regulation of heart rate is mediated largely by direct cAMP modulation of I_h channels (DiFrancesco, 1993). Our results suggest that the cardiac HCN2 channel is not essential for this type of autonomic control of cardiac activity.

Reduced I_h in $HCN2^{-/-}$ sinoatrial node cells

Using whole-cell voltage clamp recordings, we measured I_h in isolated sinoatrial node cells (Figure 6C and D). The amplitude of I_h in HCN2 knockout sinoatrial cells was reduced by ~30% (range 28–35%) compared with wild-type cells in the potential range evaluated (–90 to –140 mV, $P < 0.05$ for all potentials; no difference in mean cell capacitance between both groups). Additional recordings

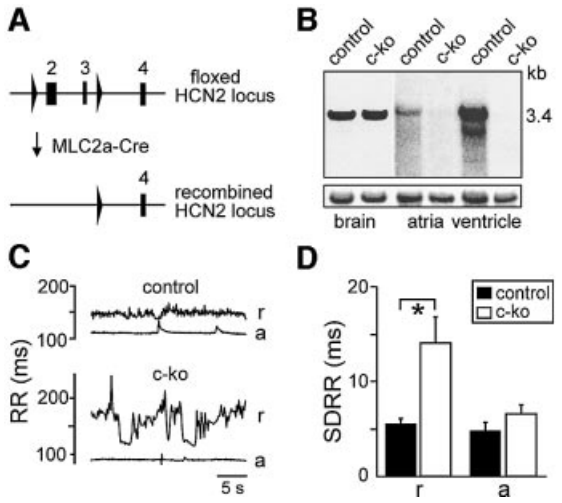

Fig. 7. Generation and analysis of heart-specific HCN2 knockout mice. (**A**) Heart-specific expression of Cre-recombinase under the control of the MLC2a promoter results in the deletion of HCN2 exons 2 and 3 in cardiomyocytes. (**B**) Top: tissue specificity of Cre- mediated HCN2 disruption. Northern blot analysis using total RNA from brain, heart atria and ventricle of cardiomyocyte-specific HCN2 knockouts ('c-kos'; $HCN2^{-/L2}$; MLC2a-$Cre^{tg/0}$) and control ($HCN2^{-/L2}$; $MLC2a^{0/0}$) animals. Blots were hybridized with a probe directed against HCN2. Bottom: blots hybridized with a β-actin probe to verify equal loading of RNA. (**C**) Representative plots of RR intervals determined by telemetric ECG recordings. Measurements were done in cardiomyocyte-specific knockout ($HCN2^{-/L2}$; MLC2a-$Cre^{tg/0}$) and control mice ($HCN2^{+/L2}$; MLC2a-$Cre^{tg/0}$) at rest (r) and during spontaneous physical activity (a). (**D**) Standard deviation of RR intervals (SDRR) obtained from 30 s ECG recordings in resting (r) and active (a) mice ($n = 5$ for each group).*$P < 0.05$.

on the selected population of sinoatrial spindle cells representing the predominant pacemaking cell type in the sinoatrial node (Mangoni and Nargeot, 2001; Wu *et al.*, 2001) revealed a similar reduction of I_h. The voltage dependence of I_h activation was not different between $HCN2^{-/-}$ and wild-type cells (see Supplementary figure 1 available at *The EMBO Journal* Online). I_h in sinoatrial node cells of wild-type mice activated significantly more rapidly compared with $HCN2^{-/-}$ mice. For example, at –110 mV, τ_{act} was 1014 ± 84 ms ($n = 49$) and 1347 ± 120 ms ($n = 42$) for wild-type and $HCN2^{-/-}$ mice, respectively. These results are in line with the significantly slower activation kinetics of heterologously expressed HCN4 compared with HCN2 channels. Taken together, these findings support the notion that I_h in sinoatrial node cells is generated by co-expressed HCN2 and HCN4 channels.

Remarkably, I_h from mutant sinoatrial node cells was increased by cAMP and reached nearly the current level of cAMP-stimulated wild-type cells (Figure 6C). For example, current amplitudes at –110 mV under control conditions were 395 ± 40 pA for wild-type ($n = 58$) and 290 ± 30 for $HCN2^{-/-}$ ($n = 60$) cells. In the presence of cAMP, current amplitudes at –110 mV were significantly increased to 490 ± 55 pA for wild-type ($n = 28$) and 430 ± 30 pA for $HCN2^{-/-}$ ($n = 22$) cells. Similarly, the activation kinetics of I_h from $HCN2^{-/-}$ cells was significantly accelerated by cAMP to the range of cAMP-stimulated wild-type cells [τ_{act} at –110 mV in the presence of cAMP: 972 ± 97 ms ($n = 22$) and 836 ± 72 ms ($n = 25$) for knockout and wild-type cells, respectively]. These results correspond with the *in vivo* ECG data and corroborate the finding that HCN2 contributes to cardiac pacemaking activity mainly under non-stimulated conditions.

Hyperpolarized maximum diastolic potential of $HCN2^{-/-}$ sinoatrial cells and sinoatrial node dysfunction

Based on our results indicating that HCN2 determines the resting membrane potential of neurons, we obtained action potential recordings from isolated sinoatrial node cells (Figure 6E). The maximum diastolic potential of HCN2-deficient sinoatrial node cells was 5 mV more hyperpolarized than that of wild-type cells (–59 ± 1 mV for $HCN2^{+/+}$ mice; –64 ± 1 mV for $HCN2^{-/-}$ mice; $P < 0.002$). To obtain direct evidence for a dysfunction of the sinoatrial node in $HCN2^{-/-}$ mice, we measured the beating of isolated heart atria. Atria from mutant mice displayed significant arrhythmic beating as compared with wild-type animals under standard conditions (Figure 6F), indicating that the dysrhythmia is caused by an endogenous dysfunction of the sinoatrial node. Taken together, these results suggest that the more negative maximum diastolic potential caused by the loss of HCN2 channels in sinoatrial node cells contributes to the observed dysfunction of cardiac pacemaking in mutant mice.

The arrhythmic beating of isolated HCN2 knockout atria could be converted to regular beating by application of 10 μM isoproterenol (Figure 6F). This is in accordance with whole-animal ECG data (Table I) and supports the notion that HCN2 is involved in the pacemaking mechanism of sinoatrial cells predominantly at a low sympathetic tone.

Mice with a cardiomyocyte-specific deletion of HCN2 display the same sinus dysrhythmia as mice lacking HCN2 globally

The arrhythmic beating of isolated $HCN2^{-/-}$ atria indicates that the dysrhythmia of mutant mice is due to sinoatrial node dysfunction. To exclude the possibility that the dysrhythmia observed in the whole-animal studies may be caused by neuronal defects leading to, for example. respiratory differences between wild-type and knockout mice, we generated mice with a cardiomyocyte-specific deletion of HCN2. We used the mouse line MLC2a-Cre expressing Cre recombinase under the control of the atrial myosin light chain (MLC2a) gene promoter. These mice allow for the excision of loxP-flanked DNA segments specifically in atrial and ventricular myocytes (Figure 7A; Wettschureck *et al.*, 2001; Wegener *et al.*, 2002). By crossing MLC2a-Cre mice with lacZ reporter mice, we confirmed that Cre-mediated recombination occurs selectively and with high efficiency in the myocardium. Sections through the sinoatrial node demonstrated near 100% recombination efficiency in sinoatrial myocytes (data not shown). Crossing of mice bearing floxed HCN2 alleles with mice carrying the MLC2a-Cre transgene (Figure 7A) led to mice lacking HCN2 channels completely in heart ventricle and atria ('c-ko'; Figure 7B). As expected, the HCN2 expression level in brain was unchanged between c-ko and control animals. Both groups of animals were indistinguishable in gross appearance, weight and spontaneous behaviour. Telemetric ECG recordings revealed

that c-ko mice displayed the same ECG pattern indicative of sinoatrial dysrhythmia as HCN2$^{-/-}$ mice. C-ko animals had highly variable RR intervals, whereas littermatched control mice displayed regular beating (Figure 7C and D; $n = 5$ for both c-ko and control group). As observed in HCN2$^{-/-}$ animals, the dysrhythmia of c-ko animals disappeared during episodes of increased physical activity. The extent of the dysrhythmia was not different between c-ko and HCN2$^{-/-}$ mice (SDRR values: 14.0 ± 3 ms for c-ko mice; 17 ± 1 ms for HCN2$^{-/-}$ mice; $P = 0.3$). These results strongly indicate that the dysrhythmia of mutant mice is produced by a cardiac-specific malfunctioning of the sinoatrial node and is not caused by neuronal deficits.

Conclusions

Hyperpolarization-activated cation currents have been suggested to play diverse physiological roles. This diversity is mirrored in the existence of four HCN channel genes with similar structure, but distinct biophysical properties and expression profiles. Our results provide evidence for the physiological role of the HCN2-encoded component of the I_h current. HCN2 critically determines the resting membrane properties of a variety of excitable cells. Our finding that the loss of HCN2 does not abolish the spontaneous activity of cardiac pacemaking cells strongly supports the idea that pacemaking is a multifactorial mechanism relying on the interaction of several currents (including the current generated by HCN4 channels). Nevertheless, the normal regularity of the rhythmic activity of pacing cells is severely disturbed by the deletion of HCN2. These findings indicate that the determination of resting membrane properties by HCN2 in these cells constitutes an important factor in the control of physiological pacemaking.

In the thalamocortical system, the loss of HCN2 facilitates oscillatory burst firing in thalamic relay neurons and associated SWDs typical of absence seizures. Thus, it is tempting to speculate that defects in HCN2 channel function may lead to absence epilepsy and sinoatrial node dysfunction in humans.

Materials and methods

All data are expressed as mean ± SEM. Statistical comparisons were carried out with Student's *t*-test or the Mann–Whitney *U* test as appropriate.

Generation of HCN2-deficient mice

The generation of mice lacking HCN2 channels globally is described in the Supplementary data.

Analysis of HCN subunit expression

A northern blot containing 7.5 μg of brain mRNA was hybridized with a probe corresponding to amino acids 176–378 of mHCN2 and probes against β-actin, mHCN1, mHCN3 and mHCN4 (Ludwig *et al*., 1998; Moosmang *et al*., 1999). Western blotting was carried out with brain membranes prepared essentially as described previously (Ludwig *et al*., 1997) using an antibody against amino acids 829–846 of mHCN2. *In situ* hybridization was done as described (Moosmang *et al*., 1999). Relative quantitative analysis of mRNA levels was accomplished by phosphor-imaging radiolabelled sections with a BAS-1500 (Fuji) and evaluating images with AIDA software. Ethosuximide was administered chronically in the drinking water (750 mg/kg/day) to 3-week-old mice over 4 weeks.

Whole-cell patch clamp analysis of neurons

Whole-cell voltage clamp recordings were made at room temperature on thalamocortical neurons of the dorsolateral geniculate nucleus and CA1 pyramidal cells of the hippocampus in coronal slices from 15- to 30-day-old mice. Slices were bathed in standard artificial cerebrospinal fluid containing 125 mM NaCl, 3 mM KCl, 1 mM NaH_2PO_4, 22 mM $NaHCO_3$, 2 mM $MgSO_4$, 2 mM $CaCl_2$, 10 mM dextrose pH 7.4 with 95% O_2/5% CO_2 (pCa 2.72). Patch electrodes were filled with 95 mM K-gluconate, 20 mM K_3-citrate, 10 mM NaCl, 10 mM HEPES, 1 mM $MgCl_2$, 0.5 mM $CaCl_2$, 1 mM BAPTA, 3 mM Mg-ATP, 0.5 mM Na-GTP pH 7.3 with KOH (pCa 6.45). Since cell capacitances of wild-type and HCN2$^{-/-}$ thalamocortical ($n = 14$ and 21, respectively) and CA1 pyramidal ($n = 11$ and 13) neurons were not significantly different, current amplitudes were not normalized for cell size. Details of I_h analysis are described in the Supplementary data.

Behavioural analysis

Locomotion of 3- to 8-month-old male mice was tested in complete darkness over 30 min in an open-field system equipped with two infrared sensor rings.

EEG recordings

Four electrodes were implanted epidurally and two in the neck muscle for EEG and EMG recordings, respectively. After recuperation, signals were recorded continuously during the first 4 h after light onset and within the first hour after i.p. injection of phosphate-buffered saline (PBS) or 200 mg/kg ethosuximide at dark onset. Signals were band-pass filtered and analysed using 4 s epochs. Absence epilepsy was characterized by generalized SWDs of at least twice the background EEG signal accompanied by low muscle activity.

Two-photon calcium imaging

Horizontal slices comprising ventrobasal thalamic complex were loaded using an injection protocol with Oregon green BABTA-AM. To induce spontaneous activity, extracellular $MgSO_4$ concentration was reduced to 0.8 mM, and 10 μM 4-aminopyridine was applied. Fluorescence was recorded using the movie mode of the imaging system (Fluoview, Olympus) at 10 Hz frequency and was analysed using the custom-made software FastAnalysis. Autocorrelograms were calculated from ~2 min long recordings. Cell activity was considered oscillatory if the autocorrelogram showed more than two satellite peaks.

Telemetric ECG recordings

ECG telemetry monitoring was done using radio frequency transmitters (TA10EA-F20, Data Sciences International) implanted in the intraperitoneal cavity with subcutaneous leads in lead II position. After 1 week of recovery, data were sampled every 20 min in freely moving mice. RR intervals and waveform characteristics were measured from four representative 30 s ECGs. Activity data provided by the telemetry system were used to determine the behavioural state of animals (rest and high activity; 0 and >4 counts/min, respectively). On three consecutive days, animals were injected i.p. with 0.9% saline (20 ml/kg) as vehicle control followed by isoproterenol (0.1 mg/kg, day 1), atropine (1 mg/kg, day 2) and methoxamine (6 mg/kg, day 3). ECGs were recorded continuously for 60 min before and after each injection.

Electrophysiological recordings of sinoatrial node cells

Isolated sinoatrial node cells were prepared from adult mice basically as described (Mangoni and Nargeot, 2001). Single sinoatrial node cells were plated onto glass coverslips. For whole-cell patch clamp recordings, the following solutions were used: bath solution, 120 mM NaCl, 20 mM KCl, 1 mM $MgCl_2$, 2 mM $CaCl_2$, 10 mM HEPES, 10 mM glucose, 2 mM $BaCl_2$, 2 mM $MnCl_2$, 0.3 mM $CdCl_2$ pH 7.4 (pCa 5.7); and pipette solution, 10 mM NaCl, 30 mM KCl, 90 mM K-Asp, 1 mM $MgSO_4$, 10 mM HEPES, 5 mM EGTA, 3 mM Mg-ATP pH 7.4 (calcium-free). Action potentials were recorded using the perforated patch technique with the following solutions: bath, Tyrode solution; and pipette solution, 10 mM NaCl, 130 mM K-Asp, 0.05 mM $CaCl_2$, 2 mM Mg-ATP, 0.1 mM Na-GTP, 7 mM creatinine phosphate, 10 mM HEPES, 200 μg/ml amphotericin B pH 7.2. All recordings were obtained at room temperature. Signals were acquired using an Axopatch 200B amplifier and pClamp software.

Isolated heart atria

Atria were connected to an isometric force transducer in an organ bath containing modified Krebs–Henseleit solution: 118 mM NaCl, 5 mM KCl, 2 mM $CaCl_2$, 1 mM $MgSO_4$, 1 mM KH_2PO_4, 25 mM $NaHCO_3$, 10 mM glucose, 0.3 mM ascorbic acid pH 7.4 with 95% O_2/5% CO_2 at 35°C. The preparation was allowed to equilibrate for 60 min.

Cardiomyocyte-specific deletion of HCN2

HCN2 knockout mice were crossed with transgenic MLC2a-Cre mice ($MLC2a^{tg/0}$) to obtain double heterozygous mice ($HCN2^{+/-}$; $MLC2a^{tg/0}$). These animals were crossed with mice homozygous for the floxed HCN2 allele ($HCN2^{L2/L2}$) to generate mice with a cardiomyocyte-specific deletion of HCN2 ($HCN2^{L2/-}$; $MLC2a^{tg/0}$).

Supplementary data

Supplementary data are available at *The EMBO Journal* Online.

Acknowledgements

We thank Astrid Vens and Anna Klein for excellent technical support, and Andrea Gerstner for help with ES cell culture. Research was supported by grants from the Deutsche Forschungsgemeinschaft and Fond der Chemischen Industrie.

References

Avoli,M., Louvel,J., Kurcewicz,I., Pumain,R. and Barbarosie,M. (1996) Extracellular free potassium and calcium during synchronous activity induced by 4-aminopyridine in the juvenile rat hippocampus. *J. Physiol.*, **493**, 707–717.

Clapham,D.E. (1998) Not so funny anymore: pacing channels are cloned. *Neuron*, **21**, 5–7.

DiFrancesco,D. (1993) Pacemaker mechanisms in cardiac tissue. *Annu. Rev. Physiol.*, **55**, 455–472.

Huguenard,J.R. (1999) Neuronal circuitry of thalamocortical epilepsy and mechanisms of antiabsence drug action. In Delgado-Escueta,A.V., Wilson,W.A., Olsen,R.W. and Porter,R.J. (eds), *Jasper's Basic Mechanisms of the Epilepsies.* Lipincott Williams and Wilkins, Philadelphia, PA, pp. 991–999.

Huguenard,J.R. and Prince,D.A. (1994) Intrathalamic rhythmicity studied *in vitro*: nominal T-current modulation causes robust antioscillatory effects. *J. Neurosci.*, **14**, 5485–5502.

Irisawa,H., Brown,H.F. and Giles,W. (1993) Cardiac pacemaking in the sinoatrial node. *Physiol. Rev.*, **73**, 197–227.

Ishii,T.M., Takano,M., Xie,L.H., Noma,A. and Ohmori,H. (1999) Molecular characterization of the hyperpolarization-activated cation channel in rabbit heart sinoatrial node. *J. Biol. Chem.*, **274**, 12835–12839.

Kim,D., Song,I., Keum,S., Lee,T., Jeong,M.J., Kim,S.S., McEnery,M.W. and Shin,H.S. (2001) Lack of the burst firing of thalamocortical relay neurons and resistance to absence seizures in mice lacking α_{1G} T-type Ca^{2+} channels. *Neuron*, **31**, 35–45.

König,P. (1994) A method for the quantification of synchrony and oscillatory properties of neuronal activity. *J. Neurosci. Methods*, **54**, 31–37.

Lacinova,L., Klugbauer,N. and Hofmann,F. (2000) Regulation of the calcium channel α(1G) subunit by divalent cations and organic blockers. *Neuropharmacology*, **39**, 1254–1266.

Ludwig,A., Flockerzi,V. and Hofmann,F. (1997) Regional expression and cellular localization of the α1 and β subunit of high voltage-activated calcium channels in rat brain. *J. Neurosci.*, **17**, 1339–1349.

Ludwig,A., Zong,X., Jeglitsch,M., Hofmann,F. and Biel,M. (1998) A family of hyperpolarization-activated mammalian cation channels. *Nature*, **393**, 587–591.

Ludwig,A., Zong,X., Stieber,J., Hullin,R., Hofmann,F. and Biel,M. (1999) Two pacemaker channels from human heart with profoundly different activation kinetics. *EMBO J.*, **18**, 2323–2329.

Luthi,A. and McCormick,D.A. (1998) H-current: properties of a neuronal and network pacemaker. *Neuron*, **21**, 9–12.

Mangoni,M.E. and Nargeot,J. (2001) Properties of the hyperpolarization-activated current (I_f) in isolated mouse sino-atrial cells. *Cardiovasc. Res.*, **52**, 51–64.

Mao,B.Q., Hamzei-Sichani,F., Aronov,D., Froemke,R.C. and Yuste,R. (2001) Dynamics of spontaneous activity in neocortical slices. *Neuron*, **32**, 883–898.

Martin,R.L., Lee,J.H., Cribbs,L.L., Perez-Reyes,E. and Hanck,D.A. (2000) Mibefradil block of cloned T-type calcium channels. *J. Pharmacol. Exp. Ther.*, **295**, 302–308.

McCormick,D.A. and Bal,T. (1997) Sleep and arousal: thalamocortical mechanisms. *Annu. Rev. Neurosci.*, **20**, 185–215.

McCormick,D.A. and Pape,H.C. (1990) Properties of a hyperpolarization-activated cation current and its role in rhythmic oscillation in thalamic relay neurones. *J. Physiol.*, **431**, 291–318.

Meeren,H.K., Pijn,J.P., Van Luijtelaar,E.L., Coenen,A.M. and Lopes da Silva,F.H. (2002) Cortical focus drives widespread corticothalamic networks during spontaneous absence seizures in rats. *J. Neurosci.*, **22**, 1480–1495.

Mellor,J., Nicoll,R.A. and Schmitz,D. (2002) Mediation of hippocampal mossy fiber long-term potentiation by presynaptic I_h channels. *Science*, **295**, 143–147.

Miake,J., Marban,E. and Nuss,H.B. (2002) Gene therapy: biological pacemaker created by gene transfer. *Nature*, **419**, 132–133.

Moosmang,S., Biel,M., Hofmann,F. and Ludwig,A. (1999) Differential distribution of four hyperpolarization-activated cation channels in mouse brain. *Biol. Chem.*, **380**, 975–980.

Moosmang,S., Stieber,J., Zong,X., Biel,M., Hofmann,F. and Ludwig,A. (2001) Cellular expression and functional characterization of four hyperpolarization-activated pacemaker channels in cardiac and neuronal tissues. *Eur. J. Biochem.*, **268**, 1646–1652.

Noebels,J., Fariello,R., Jobe,P., Lasley,S. and Marescaux,C. (1997) Genetic models of generalized epilepsy. In Pedley,J. and Pedley,T. (eds), *Epilepsy: A Comprehensive Textbook*. Lipincott-Raven, Philadelphia, PA, pp. 457–465.

Noma,A. (1996) Ionic mechanisms of the cardiac pacemaker potential. *Jap. Heart J.*, **37**, 673–682.

Pape,H.-C. (1996) Queer current and pacemaker: the hyperpolarization-activated cation current in neurons. *Annu. Rev. Physiol.*, **58**, 299–327.

Santoro,B., Liu,D.T., Yao,H., Bartsch,D., Kandel,E.R., Siegelbaum,S.A. and Tibbs,G.R. (1998) Identification of a gene encoding a hyperpolarization-activated pacemaker channel of brain. *Cell*, **93**, 717–729.

Santoro,B., Chen,S., Luthi,A., Pavlidis,P., Shumyatsky,G.P., Tibbs,G.R. and Siegelbaum,S.A. (2000) Molecular and functional heterogeneity of hyperpolarization-activated pacemaker channels in the mouse CNS. *J. Neurosci.*, **20**, 5264–5275.

Satoh,T.O. and Yamada,M. (2002) Multiple inhibitory effects of zatebradine (UL-FS 49) on the electrophysiological properties of retinal rod photoreceptors. *Pflugers Arch.*, **443**, 532–540.

Seidenbecher,T. and Pape,H.C. (2001) Contribution of intralaminar thalamic nuclei to spike-and-wave-discharges during spontaneous seizures in a genetic rat model of absence epilepsy. *Eur. J. Neurosci.*, **13**, 1537–46.

Seifert,R., Scholten,A., Gauss,R., Mincheva,A., Lichter,P. and Kaupp, U.B. (1999) Molecular characterization of a slowly gating human hyperpolarization-activated channel predominantly expressed in thalamus, heart and testis. *Proc. Natl Acad. Sci. USA*, **96**, 9391–9396.

Shinagawa,Y., Satoh,H. and Noma,A. (2000) The sustained inward current and inward rectifier K^+ current in pacemaker cells dissociated from rat sinoatrial node. *J. Physiol.*, **523**, 593–605.

Steriade,M. (2000) Corticothalamic resonance, states of vigilance and mentation. *Neuroscience*, **101**, 243–276.

Steriade,M., McCormick,D.A. and Sejnowski,T.J. (1993) Thalamocortical oscillations in the sleeping and aroused brain. *Science*, **262**, 679–685.

Thompson,G.A., Leyland,M.L., Ashmole,I., Sutcliffe,M.J. and Stanfield,P.R. (2000) Residues beyond the selectivity filter of the K^+ channel Kir2.1 regulate permeation and block by external Rb^+ and Cs^+. *J. Physiol.*, **526**, 231–240.

Vassalle,M. (1995) The pacemaker current (I_f) does not play an important role in regulating SA node pacemaker activity. *Cardiovasc. Res.*, **30**, 309–310.

Wegener,J.W., Nawrath,H., Wolfsgruber,W., Kuhbandner,S., Werner,C., Hofmann,F. and Feil,R. (2002) cGMP-dependent protein kinase I mediates the negative inotropic effect of cGMP in the murine myocardium. *Circ. Res.*, **90**, 18–20.

Wettschureck,N., Rutten,H., Zywietz,A., Gehring,D., Wilkie,T.M., Chen,J., Chien,K.R. and Offermanns,S. (2001) Absence of pressure overload induced myocardial hypertrophy after conditional inactivation of $G\alpha q/G\alpha 11$ in cardiomyocytes. *Nat. Med.*, **7**, 1236–1240

Wickman,K., Nemec,J., Gendler,S.J. and Clapham,D.E. (1998) Abnormal heart rate regulation in GIRK4 knockout mice. *Neuron*, **20**, 103–114.

Wu,J., Schuessler,R.B., Rodefeld,M.D., Saffitz,J.E. and Boineau,J.P. (2001) Morphological and membrane characteristics of spider and spindle cells isolated from rabbit sinus node. *Am. J. Physiol. Heart Circ. Physiol.*, **280**, H1232–H1240.

Received May 16, 2002; revised October 24, 2002; accepted November 19, 2002